Electroactive organically modified mesoporous silicates on graphene oxide-graphite 3D architectures operating with electron-hopping for high rate energy storage

Jianren Wang, Neus Vila, Alain Walcarius

Electroactive Organically Modified Mesoporous Silicates on Graphene oxide-Graphite 3D Architectures Operating with Electron-Hopping for High Rate Energy Storage

Jianren Wang, Neus Vilà, Alain Walcarius*

Université de Lorraine, CNRS, LCPME, F-54000 Nancy, France

* Corresponding author (AW). E-mail: alain.walcarius@univ-lorraine.fr; address: Laboratoire de Chimie Physique et Microbiologie pour les Matériaux et l'Environnement (LCPME), UMR 7564 CNRS-Université de Lorraine, 405 rue de Vandoeuvre, 54600 Villers-lès-Nancy, France.

Abstract

Pseudo-capacitive materials operating with electron-hopping as the charge transfer mechanism are elaborated by the extensive assembly of fixed redox molecules onto the surface of graphene-supported mesoporous silica film. Various physico-chemical techniques are used to characterize the resulting composites. The obtained GO@Fc-MS electrode (ferrocene functionalized silica film coated onto electro-exfoliated graphene) can deliver a specific capacity of 196 mC cm^{-2} (326 mF cm^{-2}) at a current density of 2 mA cm^{-2} and a 69% capacity retention even at 3800 C, which is much better than the traditional faradic materials. The electrochemical analyses reveal the energy storage behavior of GO@Fc-MS is a fast surface-controlled redox process. The electrode can be assembled into an asymmetric device which exhibits excellent cycling stability (no noticeable fading after 10 000 cycles) and competitive energy densities (respectively 17.7 or 9.2 µWh cm^{-2} at power densities of 0.53 or 13.7 mW cm^{-2}). These results open up new opportunities for pseudocapacitive materials based on electroactive inorganic frameworks bearing surface-tethered molecular redox sites with high energy storage capability.

Keywords: Graphene electrode; redox-active mesoporous silica film; ferrocene; energy storage material; electron hopping.

1. Introduction

Improved energy storage devices with higher energy density, better rate capability and prolonged lifespan are ever urgently needed for the keep surging demands. Supercapacitors featuring high power density and short charge-discharge time appear as a competitive candidate [1-2]. Two types of materials (i.e., carbonaceous or related electrically conductive materials and faradic materials) with their respective advantages and limitations are typically used as the electrodes. Carbonaceous materials own large surface area and good conductivity, but charges can be stored only through physical accumulation at the electrode-electrolyte interfaces (double-layer process), restricting their energy density which can be somewhat improved by using nanomaterials [1-4]. By contrast, faradic materials can store more charges through faradic reactions, but the slow reaction rates (both in terms of electron transfer kinetics or diffusional limitations) restrict their power output, even if some strategies are proposed to improve the performance of such so-called pseudocapacitive materials [5,6].

Graphene, a kind of sp^2 hybrid 2D carbonaceous materials, features large surface area (~2630 m^2 g^{-1}), excellent electrical conductivity (~10^4 S cm^{-1}), and robust mechanical properties (Young's modulus of ~1TP), being deemed as a competitive candidate for the next generation energy storage material [7]. Currently, one of the research hotspots is to couple it with faradic materials to further enhance its energy density, but at the expense of much slower chemical redox reactions, leading to deteriorated power output [8]. Two main reasons account for the slow redox reaction rate of the traditional faradic materials are: 1) the sluggish charges transfer kinetics caused by their isolating natures (e.g., ~10^{-5}–10^{-6} S cm^{-1} for nickel oxide/hydroxide, for instance [9]) and high redox activation barriers [10]; 2) the slow counter ions diffusion rate during the charges compensation process (e.g., diffusion coefficient of ~10^{-11} cm^2 s^{-1} for protons in nickel hydroxide [11]). As such, constructing a new type of graphene hybrid where the redox reaction rate of faradic part is comparable to that of electrical double layers process would be of great help to break this longtime dilemma.

The covalent bonding of mono/few layers of redox molecules on the surface of carbonaceous materials has gained more and more research interest in the energy storage field [12,13], as the artificial redox-active layer could undergo fast redox reaction, keeping a surface-controlled redox behavior even at a scan rate as high as 1 V s^{-1} [14]. Electro-grafting is a powerful way to achieve such functionalization via the electrochemical reduction of aryldiazonium derivatives [15] to generate aryl radicals which can covalently bond to the surface of a variety of substrates including carbon electrodes [16]. The resulting organic redox-molecules attached to the electrodes offer a much better rate performance in comparison to the traditional inorganic faradic species, due to fast redox kinetics, without the need for solid-phase diffusion of counter ions, thanks to active centers directly exposed to the solution [17]. Even so, there are still drawbacks hindering the development of such molecular redox systems. First, the mono/few layers nature of redox molecules restricts the number of active

sites, and therefore limits the energy density of the composites. Although much denser oligomers or even polymers can be obtained with prolonging grafting time [18], the tightly packed molecules without proper structures would impede the counter ions diffusion to reach the underlying substrates, resulting in a decreased double-layer capacitance [19]. Besides, electro-grafting appears not so optimal to functionalize the surface of graphene (preferential reactions at the edge sites [20]), causing heterogeneous functionalization and conductivity drop [14]. Therefore, it is still challenging to get a uniform molecular coating with high amounts of redox sites, while keeping the intrinsic properties of substrates and ensuring fast ions transport without surface-blocking effects.

This may be achievable by utilizing a different electron conduction mechanism, such as electron-hopping, through which charges can directly transfer between neighboring redox molecules, even without direct (covalent) connections between them. At the condition to be close enough (i.e., a local density of redox centers large enough), surface-tethered electroactive molecules with flexible linkers can undergo fast charge transfer reactions, as reported for self-assembled monolayers [21] or large dendrimers [22,23], for instance. It is however still difficult to ensure fast transport while increasing the amount and density of redox sites in faradic materials, and the thin-film technology might be an issue [24] providing it can be adapted to the coverage of highly porous and large-area electrodes, such as graphene-based ones, without pore blocking effects.

In our group, we have developed an electrochemically assisted method for the generation of sol-gel-derived organic-inorganic thin films made of a silica framework with covalently-anchored organic groups [25]. Compared to the classical sol-gel deposition methods (i.e., based on evaporation [26]), one definite advantage of the electrochemically induced film formation is its ability to generate uniform silica coatings with thicknesses from few to tens nanometers on surfaces with very complex morphology, such as macroporous electrodes [27], metal microfibers [28] or graphene nanosheets [29], for instance. When using either hard or soft templates in the electrodeposition medium, widely open and regular porous structures can be obtained, exhibiting enhanced pore accessibility and fast mass transport issues, which can be advantageously exploited for electrochemical applications [30]. In particular, the electro-assisted self-assembly (EASA) is likely to produce vertically oriented mesoporous silica films with thicknesses ranging from tens to hundreds of nanometers on conductive substrates [31,32], offering extremely large internal surface areas easily accessible for further functionalization with redox molecules, as demonstrated for metallocene species attached via click chemistry [33,34]. The regular nanochannels formed by surfactant-assisted cooperative self-assembly can accommodate a high density of redox-active centers and the resulting organically modified silicate films are highly electroactive thanks to effective electron hopping between the adjacent spatially assembled redox molecules [35,36]. These systems thus appear promising for use as pseudocapacitive materials with good performance (energy capacity expected to be larger than electroactive monolayers and power density that should be better than the bulky all-organic redox polymers). However, our previous researches

mainly focused on mesoporous films preparation by EASA on flat substrates, such as indium tin oxide or glassy carbon electrodes for electroanalysis purposes [30,37], and paid less attention to their energy storage potential on the basis of electron-hopping mechanism for which we only demonstrated very recently a fast electron hopping process among redox molecules densely packed in a mesoporous silica film coated onto a transparent flat electrode [36]. With this in mind, one could imagine to achieve the molecular functionalization of chemically inert graphene with the aid of such mesoporous film bearing a large number of redox sites to boost its energy density without sacrificing its intrinsic properties, chemical structure, and power output. It would represent a novel strategy to increase the capacitance of graphene compared to anchoring redox moieties, monolayer functionalization or the formation of hybrid composites with polymers or inorganic phases [38-40].

Here, we thus propose to evaluate the functionalization of a graphite/graphene oxide electrode with a porous electroactive inorganic framework bearing a high density of fixed molecular redox sites in view of breaking through the capacity limit of pure graphene without sacrificing any power output. Therefore, a ferrocene functionalized mesoporous silica film was generated by EASA and subsequent click coupling on the surface of an electro-exfoliated graphite foam where few-layers graphene oxide sheets distributed on the graphite surface provide large area to grow the organic-inorganic hybrid silicate film and the three-dimensionally porous graphite skeletons offer fast internal migration channels for both electrons and counter ions. After characterization of the novel hybrid pseudocapacitive material using various physico-chemical techniques, its energy storage behavior has been evaluated and tested in an asymmetric hybrid supercapacitor device.

2. Material and method

2.1. Chemicals and reagents

Tetraethoxysilane (TEOS, 98%) and (3-chloropropyl) triethoxysilane (Cl-PTES, 97%) were purchased from the Alfa Aesar. Cetyltrimethylammonium bromide (CTAB, 99%) and sodium azide (NaN_3, 99%) were obtained from Acros. Acetonitrile (ACN, 99%), dimethylformamide (DMF, 99%) and cyclohexane (99%) were purchased from Merck. Sodium sulfate (99%), ethynylferrocene (97%), copper sulfate (99%), sodium diethyldithiocarbamate trihydrate, and HCl (37%) were purchased from Sigma-Aldrich. Sodium nitrate (99%), ascorbic acid (97%) and tetrabutylammonium bromide (TBAB, 99%) originated from Fluka. Graphite foils were purchased from Shanghai Carbon Co. Ltd. All compounds were used without further purification.

The (3-azidopropyl) triethoxysilane (AzPTES) precursor was synthesized from the reaction between (3-chloropropyl)triethoxysilane and sodium azide in the presence of tetrabutylammonium bromide [34,41]. Its preparation was achieved by adding 2.0 g Cl-PTES, 1.08 g NaN_3 and 1.29 g TBAB in 100 mL ACN, which was stirred and refluxed at 90°C for 24 h under nitrogen atmosphere. Then, the ACN solvent was removed by rotary evaporation at 80°C under a reduced pressure of 0.2 bar. The

residual mixture was suspended in cyclohexane and filtered with filter paper. The remaining cyclohexane was removed using the rotary evaporator as above and the oily AzPTES product can be finally obtained. Yield: ~1.3 g, 65 %. ^{1}H NMR (400 MHz, $CDCl_3$): δ 0.66 (t, 2H, J = 0.85 Hz), 1.21 (t, 9H, J = 6.88 Hz), 1.66-1.73 (m, 2H), 3.25 (t, 2H, J = 7.16 Hz), 3.80 (q, 6H, J = 6.88 Hz).

2.2. Preparation and modification of electrodes

The electro-exfoliated graphene oxide on graphite electrode was prepared according to a slightly modified procedure as those described in the literature [42,43]. The electro-exfoliation process was performed in 0.1 M Na_2SO_4 aqueous solution with a two electrode system, where a piece of graphite foil (0.5 cm × 1 cm) and platinum mesh (2.5 cm × 2.5 cm) were used as the working and counter electrode, respectively. The exfoliation was achieved by applying a voltage of 5 V to the graphite foil for 10 minutes and the distance between the two electrodes was 5 cm. The exfoliated graphene oxide electrode, labeled as GO, was then thoroughly washed with deionized water and dried at room temperature overnight. Besides, exfoliation times of 1 min, 5 min, 15 min were also applied to further investigate the structural evolution, and the corresponding products were labeled as GO-1 min, GO-5 min and GO-15 min, respectively.

The azide functionalized mesoporous silica film was generated onto the exfoliated graphite/graphene oxide electrode by EASA, following an original protocol (as firstly reported by our group earlier [33]), which was slightly modified here. The precursor sol solution was first prepared by adding 0.50 g TEOS, 0.42 g AzPTES and 0.47 g CTAB into 20 mL ethanol/water mixed-solvent (volume ratio 1:1), along with 0.1 M $NaNO_3$ as electrolyte. The pH of the mixture was adjusted to 3 (using 0.1 M HCl aqueous solution) and stirred for 2.5 h at room temperature to allow the hydrolysis of the (organo)silane precursors and proper solubilization of the surfactant. The GO electrode was then immersed in this solution and a potential of -1.5 V (vs. silver wire) was applied for 10 s to enable the organosilica film growth around the surfactant template. The modified electrode was rapidly removed from the solution and rinsed with water and then dried at 130°C for 2 h. The azide functionalized mesoporous silica film on exfoliated graphite/graphene oxide electrode was denoted GO@Az-MS.

Prior to derivatization with ferrocene, the GO@Az-MS electrode was dipped into an ethanol solution containing 0.1 M HCl, for 30 min, in order to remove the surfactant template (this material was labelled as "CTAB-removal GO@Az-MS"). Then, a click reaction was performed between the azido moieties located onto the silica walls and the ethynyl groups of ethynylferrocene molecules in order to introduce ferrocene in the nanochannels. Typically, several pieces of CTAB-removal GO@Az-MS were put inside a mixed-solvent medium (8 mL H_2O + 12 mL DMF) containing 3.5 mg copper sulfate, 7.5 mg ascorbic acid and 10 mg ethynylferrocene, which was left for 3 days in dark. After reaction, the electrode materials were collected and rinsed with 1 mM sodium diethyldithiocarbamate trihydrate ethanol solution to remove the remaining copper catalyst and the ferrocene functionalized mesoporous silica film on exfoliated graphite/graphene electrode (denoted GO@Fc-MS) was obtained.

2.3. Apparatus

Most Electrochemical experiments (cyclic voltammetry measurements and recording charge and discharge curves) were performed using Biologic VSP potentiostat with a three-electrode system in 1 M H_2SO_4. The as-prepared samples on graphite foil fixed with a platinum clip (GO, GO@Az-MS and GO@Fc-MS), an Ag/AgCl (3.5 M KCl) electrode and a platinum mesh, were used as the working electrode, reference and counter electrodes, respectively. The as-prepared hybrid device was tested in a two electrodes system, where GO@Fc-MS and GO electrodes were fixed with platinum clips and were immersed in 1 M H_2SO_4. The electrochemical impedance spectroscopy (EIS) measurements were conducted with a Autolab PGSTAT-300 potentiostat in a three electrodes system (as mentioned above) at the open circuit potential with frequencies ranging from 100 kHz to 0.1 Hz. (Note that several points at high-frequency region in the Nyquist plot cannot be considered due to the inductance interference).

Electrode materials have been characterized by various techniques. Scanning electron microscopy (SEM) investigation was performed with a JEOL JSM-840 apparatus equipped with an energy-dispersive X-ray (EDX) microanalyzer and high-resolution SEM micrographs have been obtained with the model JSM-IT500HR apparatus (JEOL). The thickness of the graphene oxide nanosheets are measured by processing the high resolution SEM micrographs with the software "ImageJ", which can properly measure the selected distances. After that, the thickness data are statistically processed to obtain the thickness distribution graph. X-ray Photoelectron Spectroscopy (XPS) measurements were performed using the Kratos AxisUltra DLD apparatus equipped with a monochromatic Al Kα source. Atomic force microscopy (AFM) analysis was done with Asylum MFP3D-Bio apparatus (Oxford Instrument). Raman spectroscopy measurements were carried out with a Jobin Yvon T64000 spectrometer with green light laser (514 nm). The N_2 adsorption – desorption isotherms were recorded at −196°C on Belsorp system (BEL JAPAN, INC) and the pore size distribution curves were calculated by the Barrett – Joyner – Halenda (BJH) method from the adsorption branch.

3. Results and Discussions

3.1. Electrode modification and characterization

The overall synthesis procedure to get the ferrocene grafted mesoporous silica film on exfoliated graphite/graphene oxide electrode (GO@Fc-MS) is schematically illustrated in **Fig. 1**. First of all, an efficient electro-exfoliation method is adopted to open the channels of the low-cost graphite foil and to separate the surficial graphite into few-layers of graphene oxide. Compared with the time/energy-consuming or environment-unfriendly chemical or physical graphene preparation processes, this method only takes a few minutes without harmful by-products throughout the whole process [42,43]. Subsequently, the EASA method [33] is used to generate the mesoporous silica deposits containing azide groups on the electrode surface, which is

expected to form a hierarchically porous silica/graphene oxide sandwich structure [29]. Finally, ethynylferrocene molecules acting as the redox active sites are covalently anchored on the surface of the silica wall, at the highest density compatible with fast charge transfer processes (as optimized for flat electrodes [35,36]) with the help of Cu(I)-catalyzed azide-alkyne cycloaddition (CuAAC) click reaction [33,34].

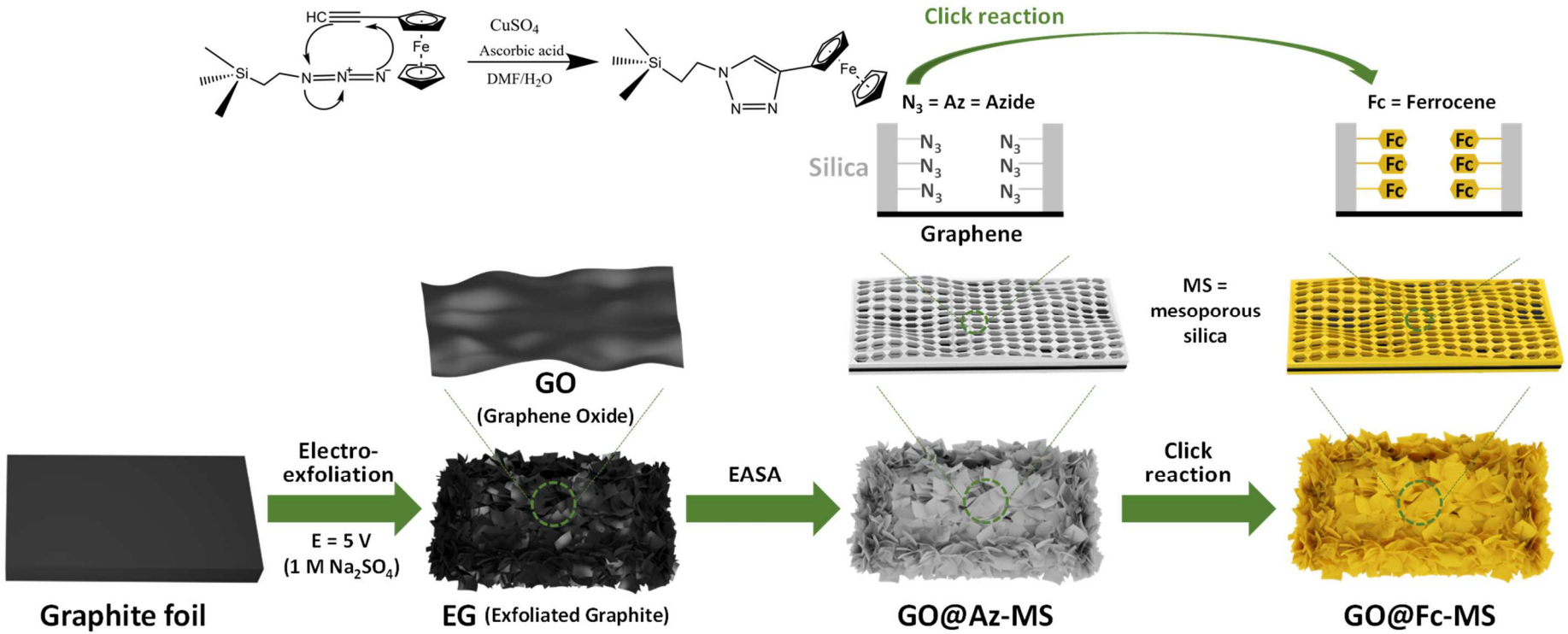

Fig. 1. Schematic illustration of the formation of GO@Fc-MS. It involves the formation of exfoliated graphite (EG) in the form of graphene oxide (GO), its modification with an azide-functionalized mesoporous silica (Az-MS) and a final derivatization by click chemistry to form the ferrocene-grafted mesoporous silica (Fc-MS).

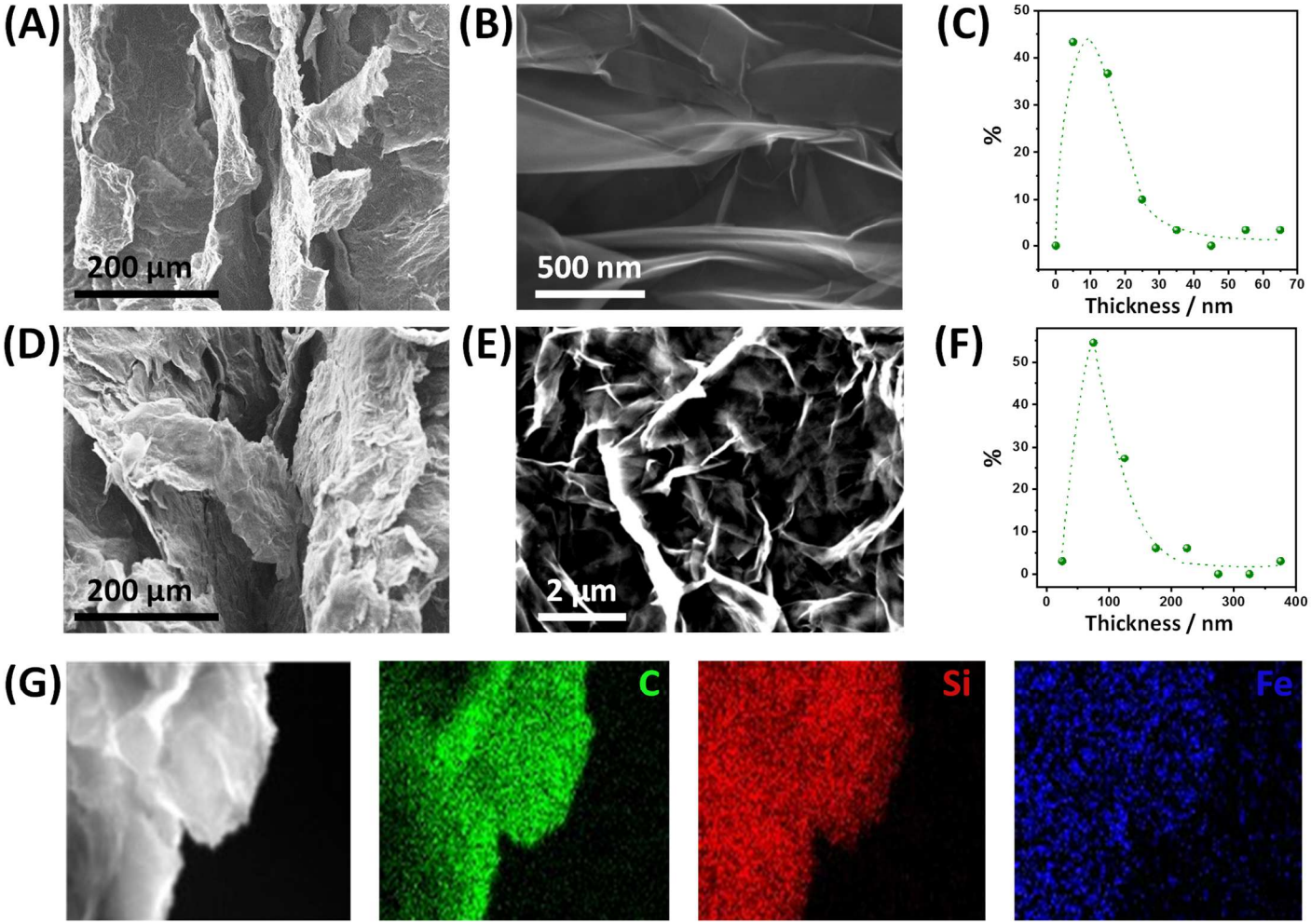

Fig. 2. (A-D) SEM examination of GO (A,B) and GO@Fc-MS (D,E) by SEM; (C,F) thickness distribution for GO (C) and GO@Fc-MS (F) on the basis of the corresponding high resolution micrographs; (G) EDS mapping results (C, Si and Fe elements) of the GO@Fc-MS material.

The morphology evolution during the preparation is analyzed by SEM. It can be seen from **Fig. S1** that the structure of pristine graphite foil is compact without obvious channels. However, after electro-exfoliation (**Fig. 2A&B**), the interlayer of graphite has been expanded and macrochannels are formed due to the swell effects of inserted SO_4^{2-} ions and in-situ generated O_2 and SO_2 gases during the electrochemical process [65]. The high-resolution SEM micrograph further reveals that the surface of the graphite skeleton is coated by numerous ultrathin nano-sheets with most of the thickness distributed at 9±6 nm, proving the formation of few-layers graphene oxide (**Fig. 2B&C**). Similarly, AFM results confirm from height profile measurements the existence of fairly flat nano-sheets (see illustration with an average thickness of 6 nm in **Fig. S2**). The exfoliation time plays an important role on the GO morphology, which can have some effects on the energy storage behavior. As shown in **Fig. S3a**, the graphite foil becomes thicker and the channels gradually expand to 780 μm as the exfoliation time reaches 10 minutes. However, the thickness of the porous layer significantly declines (to 220 μm) when further extending the exfoliation time (to 15 min), since the shedding of graphene oxide flakes into the solution becomes dominating. As the consequence, the highest current response is also observed for the 10 minutes exfoliated sample on the basis of cyclic voltammetry tests (**Fig. S3b).** After coating with a thin layer of ferrocene functionalized silica film, the morphology of GO@Fc-MS doesn't change too much, but the serious charge accumulation and some cracks on its surface indicate there is an isolating silica layer onside. (**Fig. 2D&E and Fig. S4)** Besides, compared with that of GO, the sheet thickness of GO@Fc-MS increases to about 75±15 nm (**Fig. 2F)**, which means that the thickness of the silica layer coated onside is ca. 65-70 nm. The EDS mapping results of GO@Fc-MS also show uniform distribution of the C, Si, Fe elements (**Fig. 2G)**, further confirming the rather homogenous coating of ferrocene functionalized silica layer on its surface. It should be noted that there are some mapping signals from the outside of the GO@FC-MS flake. This phenomenon, already observed in the literature [45,46], could be due to the low intensity of Fe signals on the flake, giving a relative high density of Fe noisy signals outside (the relative Fe content is only 0.58%, as estimated from EDX data (**Fig. S5**)).

To identify the structural and compositional evolution of the graphite electrode upon the various modification steps (leading to the materials GO, GO@Az-MS and GO@ Fc-MS), a series of Raman spectra is presented in **Fig. 3A&B**. The strong G band (~1580 cm^{-1}), 2D band (~2760 cm^{-1}) and negligible D band (~1360 cm^{-1}) visible for the original graphite foil (see curve (a) in Fig. 3A) indicate that it is highly graphitized with few defects [47]. By contrast, an obvious D band and a small 2G (~2920 cm^{-1}) band, corresponding to the defect signals from the edge sites of graphene, in addition to the remaining G and 2D bands of graphite can be detected for GO (see curve (b) in Fig. 3A). This proves that graphene oxide is successfully obtained through the electro-exfoliation method [43,48]. After deposition of azide functionalized silica, no significant changes except that several new peaks (marked with green stars on the images, see curves (c) in Fig. 3A&B) can be observed for GO@Az-MS, which can be ascribed to the long alkyl chain of CTAB surfactant [49,50]. Unfortunately, the typical

Raman signature for azidopropyl-grafted silica materials appearing in the 1250-1500 cm^{-1} region [51] cannot be noticed here because it is obscured by the intense D band of graphene. Nevertheless, a broad band from ~375 cm^{-1} to ~570 cm^{-1} and another one located at ~2110 cm^{-1} can be attributed to the Si–O–Si vibrational mode [50] and the antisymmetric stretching mode of azide group [52], respectively (see curve (c) in Fig. 3B), which verifies the azide functionalized silica film has been formed on the surface of graphene. The intensities of Raman signals from D and G bands significantly decrease, which means the existence of silica film on the carbon surface could block the signals. Besides, the I_D/I_G ratio (i.e., usually used to characterize graphene functionalization [53]) decreases from 0.86 of GO to 0.78 because the edge/defect sites of graphene may generate relatively thicker silica film onside during the electro-deposition process, and thus reduce more intensity of D band, owing to the well-known electrocatalytic properties of the edge sites of graphene [54]. After CTAB extraction and click coupling with ethynylferrocene, the signals from CTAB and azide disappear for GO@Fc-MS (curves (d) in Fig. 3A&B), indicating the surfactant is removed and most azide groups take part in the click reaction [55]. The I_D/I_G ratio slightly increase back to 0.81, which may due to the more beam-accessible graphene oxide/graphite surface, as the intensities of the Raman signals recover back to some extent.

XPS is further used to complete the materials characterization and to monitor semi-quantitatively the click reaction. The survey scan spectra of graphite foil, GO, GO@Az-MS and GO@Fc-MS are given in **Fig. S6a** and the detailed element ratio is given in **Table S1**. It can be seen clearly that an increment of the oxygen contents occurs, from 5.0% in graphite to 14.8% in GO, indicating the partial surface oxidation of graphite during the electro-exfoliation process. Besides, the signals from silicon, nitrogen and iron can be detected in sequence after the silica deposition and click reaction (**Fig. S6b-d**). As shown in the high resolution C_{1s} spectra (**Fig. 3C**), a band for C-O at ~287 eV and another for C(O)-O at ~288.7 eV can be detected for GO (in addition to the expected C-C and C=C signals of graphene), which constitutes an evidence for the existence of hydroxyl and carboxyl groups on the carbon surface [42]. The existence of oxygen-containing groups on the surface may facilitate the anchoring and stabilize the silica layer being deposited subsequently [48,51]. One can also see some contribution of C-N (C_{1s} signal at ~286.6 eV) after deposition of the silica film (GO@Az-MS sample), which comes from the CTAB surfactant and disappears while a new one grows at ~286.2 eV for GO@Fc-MS, indicating the effective removal of the template and the formation of 1, 2, 3-triazole group, respectively. This is seen more clearly on the high-resolution N_{1s} spectra (**Fig. 3D**). For GO@Az-MS, four contributions can be recognized: the neutral and negative nitrogen species from azide groups (401.0 eV), the positively charged nitrogen species from CTAB (402.9 eV) and azide groups (404.5 eV), as well as some residual nitrate ions originating from the electrodeposition electrolyte (406.8 eV), which are consistent with literature data for the azidopropyl moieties [56,57], the quaternary ammonium centers of CTAB [58] and nitrate [84]. After being washed with HCl/EtOH solution, both signals from CTAB and nitrate disappears, and after click

reaction with ethynylferrocene, the characteristic signals from the azide groups (at 401.0 eV and 404.5 eV, with 2:1 ratio [60]) vanishes and a new broadened peak emerges (with chemically distinct nitrogen contributions located at 400.2 eV and 401.3 eV), which corresponds to the 1,2,3-triazole groups [61]. A semi-quantitative estimation of the proportion of azido groups involved in the click reaction can be roughly obtained from comparing the ratio of azido peak at ~404.5 eV for both GO@Fc-MS (**Fig. 3D**) and GO@Az-MS after CTAB removal (**Fig. S6d**), giving rise to a yield of 82%. The presence of ferrocene on the GO@Fc-MS electrode is evidenced by the Fe_{2p} signal (**Fig. S6c**), via its two contributions, $2p_{1/2}$ and $2p_{3/2}$ transitions respectively located at 721.1 and 708.2 eV, characteristic for ferrocene [62]. Finally, trace amounts of N (0.6%) and S (1.5%) can be also observed for GO (i.e., prior to film formation), possibly due to some impurities in the graphite foil (Table S1). Some previously published works observed Pt-related impurities in products when using Pt as the counter electrode for the electro-exfoliation process [63], however this phenomenon was not evidenced here.

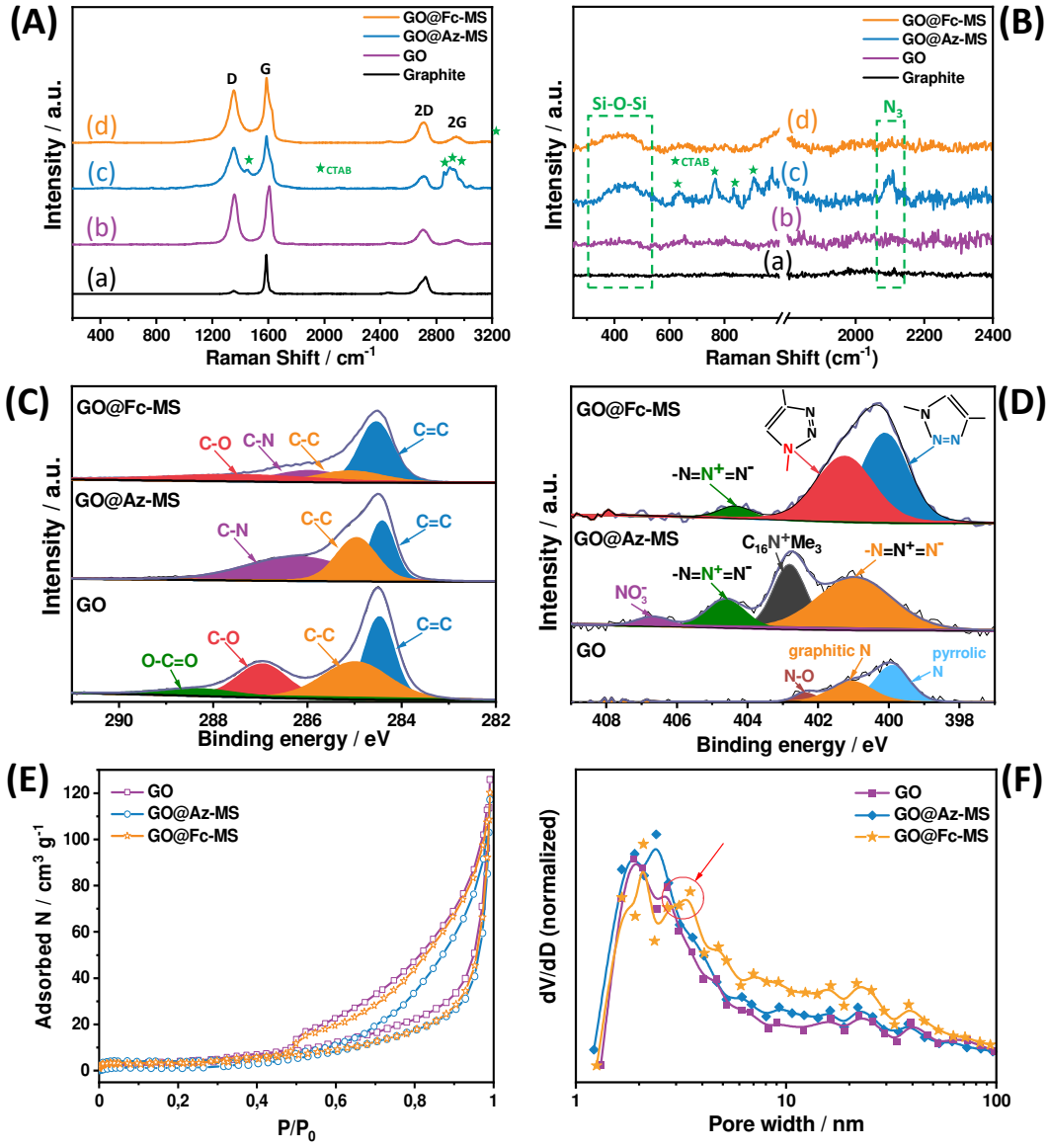

Fig. 3. (A, B) Raman spectra of the graphite foil, GO, GO@Az-MS and GO@Fc-MS; (C, D) XPS narrow spectra for C_{1s} (C), N_{1s} (D) of GO, GO@Az-MS and GO@Fc-MS; (E) N_2 adsorption-desorption and (F) pore distribution curves for the same samples.

Nitrogen adsorption-desorption isotherms for GO, GO@Az-MS and GO@Fc-MS materials are given in **Fig. 3E**. Typical IV isotherms with H_3 or H_4 hysteresis loop can be observed for the three samples, which means the existence of mesopores formed by the assembly of plate-like particles [64]. At the relatively high pressure (P/P_0>0.85), a steep increase of nitrogen adsorption amount occurs for the three samples, a sign of the existence of macropores resulting from agglomerates of graphene oxide sheets [65], consistent with the morphology observation (**Fig. 2B&E**). The corresponding pore distributions calculated from the Barret–Joyner–Halenda (BJH) model with adsorption branches are given in **Fig. 3F**. There is not too much difference for pore structure of GO and GO@Az-MS, but a new type of pores located at ~3 nm appears for GO@Fc-MS due to the removal of CTAB template, which proves the silica layer coated on the surface of graphene oxide is highly mesoporous.

3.2. Energy storage performance of the electrodes

The energy storage performance of graphite foil, GO and GO@Fc-MS are firstly compared from cyclic voltammetry experiments in 1 M H_2SO_4 aqueous electrolyte with a three-electrode setup. The CV curves of original graphite foil, GO and GO@Fc-MS, as recorded at a scan rate of 50 mV s^{-1}, are shown in **Fig. 4A**. The original graphite foil shows a negligible current response due to its compact structure and low surface area. In contrast, the GO delivers much higher current with an obvious rectangular shape, a sign of the electrical double layer capacitance, demonstrating the significantly increased active area from its porous structure and the wide effective surface area due to the presence of large amount of graphene oxide sheets. Besides, a pair of weak redox peaks located at ca. 0.38 V can be observed, which may come from the oxygen containing functional groups on the electrode surface, such as quinone/hydroquinone functions [66]. After introducing the ferrocene functionalized silica film, a pair of well-defined redox peaks originating from the reversible redox reaction of ferrocene molecules can be observed for GO@Fc-MS. Besides, the double-layer capacitance of this GO@Fc-MS electrode remains similar to that of GO in the non-faradic potential region from 0.1 V to 0.2 V, demonstrating that the existence of mesoporous silica thin film on its surface does not cause obvious resistance for electrolyte transport through the silica-on-graphene oxide layer (also true over extended potential range for the ferrocene-free GO@Fc-MS material, see **Fig. S7**, confirming further an easy access for solution species to the graphene surface even after modification). This is indeed important, also for the faradic process, as the mechanism of electron self-exchange reactions between adjacent ferrocene moieties operating here (an electron-hopping process well accepted for electroactive polymers consisting of fixed molecular redox sites [67] or surface-tethered redox molecules with flexible linkers [68], which is also valid for organic polymers with pendant ferrocenes [69]), involves charge neutralization by the electrolyte ions from the solution (Eq. 1).

$$Fc - 1\,e^- + X^-_{(sol)} \Leftrightarrow Fc^+,X^-_{(film)} \quad (1)$$

(with Fc = ferrocene; Fc^+ = ferricinium; X^- = counter-anion; sol = solution)

The highly porous structure of GO@Fc-MS thus contributes to facilitate the transport of such ions necessary to maintain charge balance, which is a key parameter in pseudo-capacitive energy storage always looking at improved ion accessibility to redox-active sites [70]. The CV curves of GO@Fc-MS recorded at various scan rates ranging from 20 mV s^{-1} to 200 mV s^{-1} (**Fig. 4B**) reveals symmetrical redox current responses with rather small cathodic-to-anodic peak potential separation (yet increasing with potential scan rates, see **Fig. S8**). This confirms the efficient charge transfer and the electrolyte transport processes of the electron-hopping system, and the presence of only a single couple of anodic and cathodic peaks indicates no electronic interaction between ferrocene centers in the nanochannels.

To further evaluate the energy storage behavior and its capacity, the charge-discharge curves of GO@Fc-MS at various current densities from 2 mA cm^{-2} to 100 mA cm^{-2} are displayed in **Fig. 4C**. Different from the triangular charge-discharge curve of double-layer capacitance, the curves are distorted but without obvious charge-discharge plateau. This phenomenon illustrates that the redox reaction of ferrocene molecules is not an ion diffusion-controlled process but a surface-controlled one. Furthermore, the nearly symmetric curves also verify the highly reversible redox reaction and the coulombic efficiencies at different current densities are all above 95% (**Fig. S9**). Based on the galvanostatic charge-discharge curves for GO (**Fig. S10**) and GO@Fc-MS (**Fig. 4C**), the specific capacities of both electrodes as a function of current density are given in **Fig. 4D**. It can be seen clearly that the GO@Fc-MS exhibits a specific capacity of 196 mC cm^{-2} (or a capacitance of 326 mF cm^{-2}) at a current density of 2 mA cm^{-2} which is almost twice that of GO (107 mC cm^{-2} or 178 mF cm^{-2}). The contribution of the faradic Fc-MS material is thus equal to 89 mC cm^{-2}, a value larger by almost two orders of magnitude than that reported for a similar ferrocene functionalized film deposited onto a flat electrode surface [54], confirming the interest of the large area and highly porous GO support. Generally, compared with double-layer materials, the faradic materials always show limited rate performance due to the slow electrons and ions transfer processes. But the electron-hopping governed redox process operating here is a very fast reaction, and the capacity of GO@Fc-MS can remain at 69% of its larger value at a current density as high as 100 mA cm^{-2} (135 mC cm^{-2} or 224 mF cm^{-2}), which is even better than the 52% observed for the purely capacitive GO electrode under the same condition. The normalized rate performance (excluding the effect of capacity) of GO@Fc-MS and some recently reported faradic materials are plotted in **Fig. 4E**. The rate performance of GO@Fc-MS is better than traditional faradic materials, with a capacity retention of 69% even at a C-rate value of 3800 h^{-1}, further demonstrating the advantage of the electron-hopping processes. Besides, as shown in **Table S2**, GO@Fc-MS also shows a competitive energy storage ability in comparison to the composites of graphene and faradic materials reported in the literature. The GO@Fc-MS also delivers a long cycle lifespan and 98% of the initial capacitance can remain after 1000 successive CV

cycles (**Fig. 4F**). Capacitance and capacity retention can also be evaluated from integrating the CV curves at various potential scan rates (**Fig. S11**), giving rise to the same conclusions as for galvanostatic experiments. Moreover, from such integration, one can estimate an amount of electrochemically accessible redox molecules of ca. 0.2 mg cm^{-2}, which represents about 80% of its total content in the film (0.25 mg cm^{-2}, as obtained from ICP chemical analysis after acidic digestion of the sample). This means the electron hopping occurs efficiently in most of the composite material volume despite the isolating properties of the silica matrix.

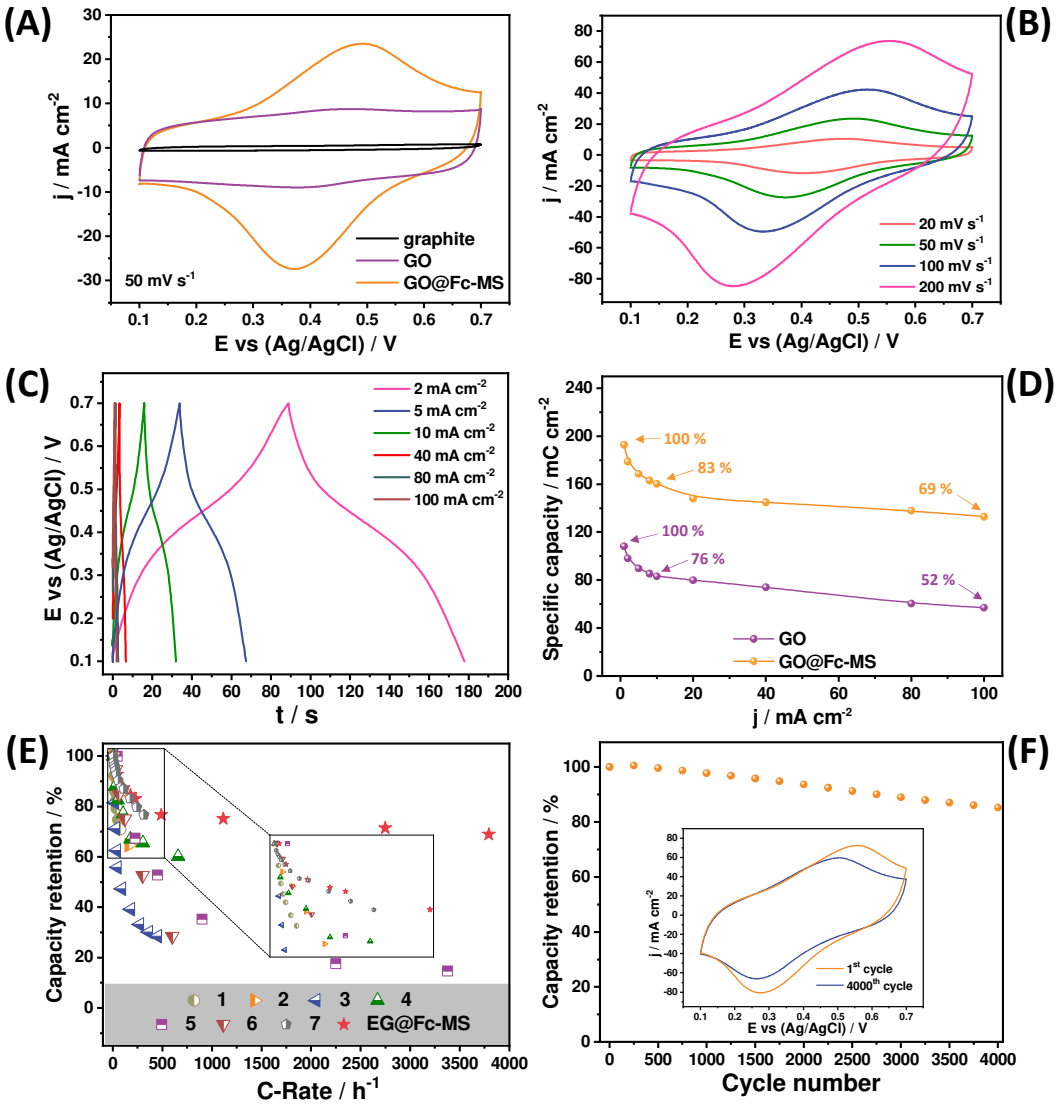

Fig. 4. Energy storage behavior of graphite, GO and GO@Fc-MS electrodes in 1 M H_2SO_4. (A) CV curves recorded for the three electrodes at a scan rate of 50 mV s^{-1}; (B) CV curves recorded for GO@Fc-MS at various potential scan rates, from 20 to 200 mV s^{-1}; (C) charge/discharge curves of GO@Fc-MS obtained at various current densities, from 2 to 100 mA cm^{-2}; (D) specific capacity of the GO and GO@Fc-MS electrodes measured at different current densities, ranging from 2 to 100 mA cm^{-2}; (E) comprehensive plots of normalized rate performance for GO@Fc-MS and several faradic materials reported in recent years (1, Ni-Mn hydroxide on carbon nanofoam; 2,

Co-Cd selenide nanorods; 3, Li_2MnO_3 nanorods; 4, Ni-Co hydroxide on carbon fibers; 5, Fe_2O_3/polypyrrole nanoarrays on carbon cloth; 6, *n*-butyllithium-treated $Ti_3C_2T_x$ MXenes; 7, amorphous Ni-Co-Mn hydroxides; the corresponding references are given at the end of the Supporting Information); (F) cycling performance of GO@Fc-MS for multiple CV measurements performed successively at a scan rate of 200 mV s^{-1}.

Electrochemical Impedance Spectroscopy (EIS) is also used to analyze the energy storage originating from the electron hopping process, in the frequency range from 100 kHz to 0.1 Hz at the open circuit potential, and the Nyquist plots for GO and GO@Fc-MS are given in **Fig. 5A**. At high frequency, the intersection point on the real axis represents the ohmic resistance of the electrolyte and the internal resistance of the electrode (R_s), which is very small and similar for both GO (0.95 Ω) and GO@Fc-MS (0.65 Ω) due to the good conductivity of the graphene oxide/graphite substrate. In the high to middle frequency region, a semi-circle indicative of the charge transfer resistance (R_{ct}) is usually observed for faradic materials [71-73], the diameter of which being as small as high are the charge transfer kinetics. Here, such charge transfer resistance is negligible (no noticeable semi-circle) not only for GO but also for GO@Fc-MS, which demonstrates a fast and efficient electron hopping process involving the redox-active ferrocene moieties attached to the material. The tail at low frequency of the Nyquist plot corresponds to the diffusion limiting process. The similar and nearly vertical lines for GO and GO@Fc-MS show both of them own fast ions diffusion and prove the coating of the silica layer on the surface of graphene oxide will not affect significantly the ions diffusion, confirming the interest of graphene oxide sheets to facilitate electrolyte penetration and pseudocapacitance [66]. The electrolyte ions diffusion coefficient (D_0) can be evaluated with the aid of equations (2) and (3):

$$D_0 = R^2T^2/2A^2n^4F^4C^2\sigma^2 \qquad (2)$$

$$Z' = R_s + R_{ct} + \sigma\omega^{0.5} \qquad (3)$$

Where D_0 is the diffusion coefficient, R is the gas constant, T is the absolute temperature, A is the electrode surface area, n is the number of electrons, F is the Faraday's constant, C is the concentration of ions, ω is the frequency, and σ is the Warburg factor which is the slope of $\omega^{-0.5}$ *vs* Z' plot.

By fitting our data (**Fig. S12**), D_0 values of 1.9×10^{-5} cm^2 s^{-1} and 1.4×10^{-5} cm^2 s^{-1} are obtained, respectively for GO@Fc-MS and GO electrodes. The similar and fast diffusion rates prove: 1) the existence of the highly porous silica film on the surface of graphene does not block the ions diffusion; 2) there is no solid diffusion process during redox reaction of ferrocene molecules, indicative of the fully solution-phase exposed active sites (contrary to what happens in insertion-based materials for instance). The phase angle variation on frequency (Bode phase plot) for GO and GO@Fc-MS is plotted in **Fig. 5B**. At the low frequency of 0.1 Hz, the phase angle can achieve -79° for both of them, suggesting a behavior much like an ideal capacitor [74]. The frequencies at the phase angle of -45° (f_0) representing the point at half-maximum capacitance are 1.70 Hz and 1.27 Hz for GO and GO@Fc-MS,

respectively, indicating that the presence of the ferrocene functionalized silica film does not affect too much the charge-discharge rate performance [75]. The corresponding time constants τ_0 ($1/f_0$), i.e. the minimum time needed to discharge all the energy with an efficiency greater than 50%, are very short: only 0.59 s for GO and 0.78 s for GO@Fc-MS, yet not at the level of purely carbon nanomaterials [76]. but satisfactory for a porous carbon electrode covered with an electroactive layer [75]. Similar τ_0 for GO and GO@Fc-MS also demonstrates the low resistance to charge transfer and ions diffusion processes in Fc-MS.

GO@Fc-MS is further analyzed by recording CV curves over a wide range of scan rates from 5 mV/s to 500 mV s^{-1} (**Fig. S13**). Its behavior can be evaluated by fitting the redox peak currents vs. scan rates with the equation of $i = av^b$, and the empirical b value is an indicator of the type of reaction. A b value of 0.5 represents a diffusion-controlled behavior (battery-type), while b value of 1 is indicative of surface-controlled charge transfer (ideal capacitive energy storage process). As shown in **Fig. 5C**, the fitting results of GO@Fc-MS approach the ideal value of 1 (0.91 in average for cathodic redox peaks and 0.88 for anodic redox peaks), over a wide range sweep rate from 5 mV s^{-1} to 500 mV s^{-1}, indicating the redox of ferrocene is mostly a fast surface-controlled reaction. In contrast to the flat electrode, besides providing more space to grow the ferrocene functionalized silica film, the use of the rough GO electrode might accelerate the counter ions diffusion by altering the diffusion mode from 2D planar diffusion to 3D spherical diffusion [77], finally resulting in a surface controlled behavior in such wide potential window. To obtain the quantitative capacitive contribution at a fixed scan rate, the CV results of GO@Fc-MS are further fitted with the following equation (4):

$$i(V) = k_1 v + k_2 v^{0.5} \qquad (4)$$

Where $k_1 v$ and $k_2 v^{0.5}$ represent the surface-controlled current and diffusion-controlled current respectively.

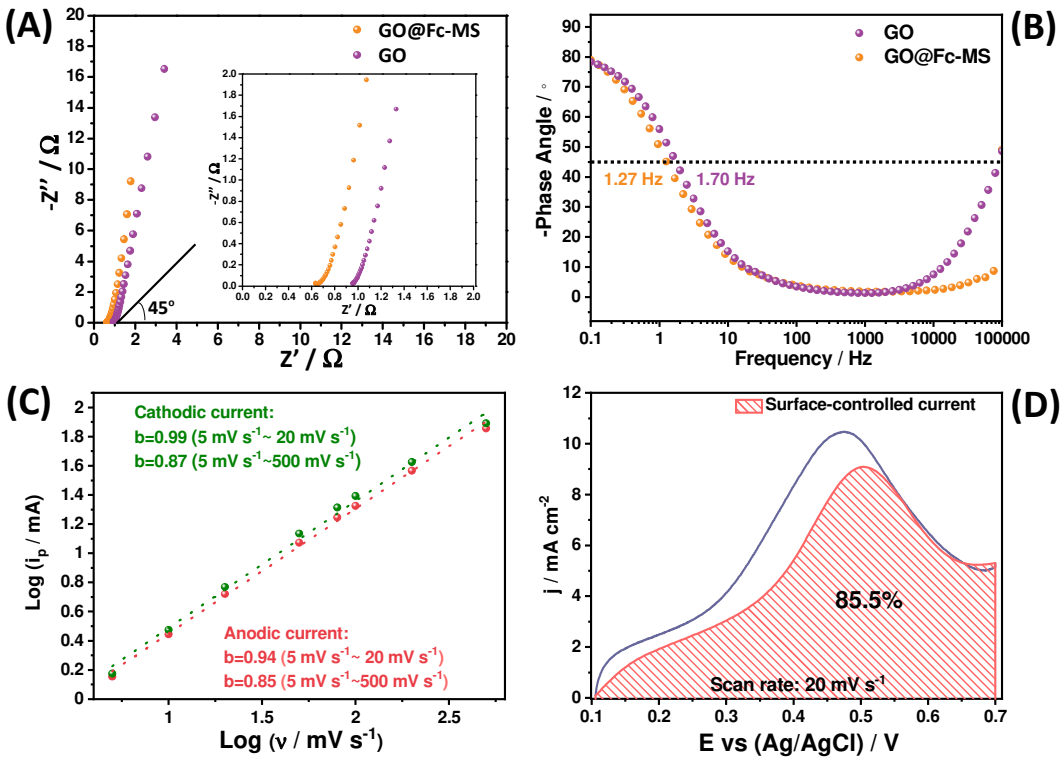

Fig. 5. (A, B) EIS data for GO and GO@Fc-MS electrodes recorded at open circuit potential in the frequency range 100 to 0.1 Hz: (A) Nyquist plots and (B) Bode phase plots; (C) Variation of CV peak currents for GO@Fc-MS as a function of the logarithm of scan rates (from 5 to 500 mV s^{-1}); (D) Ratio of the surface-controlled current of the oxidation process at the scan rate of 20 mV s^{-1} (marked by the shaded region).

The fitting result reveals that 85.5 % of the total current of the anodic peak comes from the surface-controlled process at the scan rate of 20 mV s^{-1} (**Fig. 5D**). Such high ratio for GO@Fc-MS further confirms the fast transport of counter-ions, which are not restricting the charges transfer processes by electron-hopping (Eq. 1), in contrast to conventional faradic materials (e.g. insertion or intercalation pseudocapacitors [5, 78]).

3.3. Asymmetric hybrid cell assembly

In order to show the practical potential of the GO@Fc-MS electrode, a pseudocapacitor is further assembled by employing GO@Fc-MS as anode, GO as cathode (the area ratio of GO@Fc-MS to GO is 2) and 1M H_2SO_4 as the electrolyte. Typical results are given in **Fig. 6**.

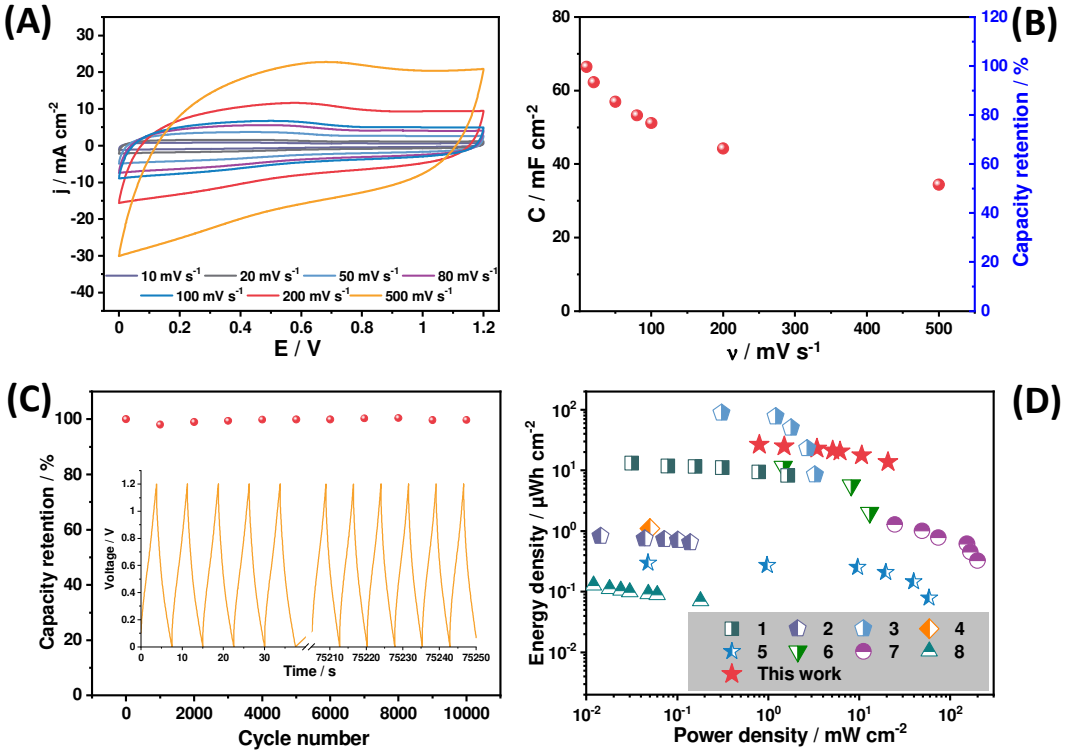

Fig. 6. The energy storage performance of GO@Fc-MS//GO hybrid pseudocapacitor in 1M H_2SO_4. (A) CV curves at various scan rates (from 10 to 500 mV s^{-1}); (B) Capacity values calculated from CV curves as a function of scan rate; (C) cycling performance at constant current density of 13.3 mA cm^{-2} (initial and final five charge-discharge curves); (D) Ragone plots of the GO@Fc-MS//GO pseudocapacitor and previously reported capacitors (1, polyethylene fibers covered by polydopamine, Ag and poly(3,4-ethylene dioxythiophene)/poly(styrenesulfonate); 2, poly(3,4-ethylene dioxy-thiophene):poly(styrenesulfonate)/ferritin nanoclusters within multiwalled carbon nanotube sheets; 3, graphene/MnO_2; 4, carbon nanotube yarns dotted with Co_3O_4 and NiO nanoparticles; 5, 3-D graphene carbon nanotube carpet; 6, actived carbon; 7, onion-like carbon; 8, Fc-MS on ITO; the corresponding references are given at the end of the Supporting Information).

As shown in **Fig. 6A**, the GO@Fc-MS//GO pseudocapacitor is able to stably work over the potential window from 0 to 1.2 V at scan rates ranging from 10 to 500 mV s^{-1}. Besides the double layer capacitance of graphene oxide, an additional pair of broad peaks originating from the redox reaction of ferrocene confirms the energy storage contribution form the faradic reaction. Different from the three-electrode configuration (used for all above experiments), the voltammetric current responses in a two-electrode system depend on the features of both working and counter electrodes, which may lead to distorted signal, especially for non-faradic materials [79]. This explains the broader peaks observed with the hybrid pseudocapacitor (**Fig. 6A**) in comparison to the GO@Fc-MS electrode (**Fig. 4B**). The specific capacitances at various scan rates are calculated from CV curves, based on the total areas of the two

electrodes (**Fig. 6B**). A capacitance of 67 mF cm^{-2} can be delivered at the scan rate of 10 mV s^{-1}, and it can still maintain 32 mF cm^{-2} (47%) at 500 mV s^{-1}, 2.4 s discharging time. In contrast to the obvious plateau of batteries, the distorted triangle charge-discharge curves reveal the pseudocapacitor nature of the GO@Fc-MS//GO device (**Fig. S14**). Ragone plots further reveal that the high energy density of 17.7 µWh cm^{-2} can be achieved at power density of 0.53 mW cm^{-2} and still remains as high as 9.2 µWh cm^{-2} at high power density of 13.7 mW cm^{-2}, being really competitive regarding recently reported supercapacitors performance (**Fig. 6D**). Besides, the cycling stability of the asymmetric supercapacitor is also determined by the galvanostatic charge-discharge curves (at current density of 13.3 mA cm^{-2}), showing no obvious capacity fading even after 10 000 successive cycles (**Fig. 6C**).

4. Conclusions

An organic-inorganic hybrid material acting as a large-scale redox junction system has been developed through covalently anchoring ferrocene molecules on a mesoporous silica thin film electrogenerated onto the surface of a graphene oxide-based electrode produced by electro-exfoliation of a graphite foil. Different from the traditional redox reactions (electrochemical insertion or intercalation), the electron-hopping mechanism operating here enables efficient and reversible transformation of surface-tethered ferrocene moieties with flexible linkers, thanks to fast charge transfer processes and low resistance to counter-ions diffusion. By further coupling with the good conductivity and large surface area of graphene oxide/graphite substrate, the GO@Fc-MS electrode exhibits a capacity of 196 mC cm^{-2} (326 mF cm^{-2}) at a current density of 2 mA cm^{-2}, of which 45% originates from the faradic Fc-MS layer. It delivers a remarkable capacity retention of 69% even at a high current density of 100 mA cm^{-2} (C-rate of 3800 h^{-1}). Finally, a pseudocapacitor (GO@Fc-MS//GO) is constructed and achieves a large energy density of 9.2 µWh cm^{-2} at a high power density of 13.7 mW cm^{-2}. This work well demonstrates the advantages of the electroactive mesoporous hybrid system consisting of a high density of molecular redox sites in terms of fast charge and mass transfer processes, high level of electroactivity and long cycling life, which may pave a new avenue on the construction of high-performance electrode materials for energy-related storage and conversion devices.

Acknowledgements

The authors are grateful to several people from LCPME for their help in the physico-chemical techniques used for characterization of the materials: C. Genois (ICP-AES), A. Renard (XPS and N_2 adsorption-desorption), M. Etienne (high resolution SEM), M. Dossot (Raman spectroscopy) and G. Francius (AFM). JW acknowledges a financial support from the China Scholarship Council for his doctoral studies.

References

[1] P. Simon, Y. Gogotsi, Materials for electrochemical capacitors. Nat. Mater. 7 (2008) 845–854. https://doi.org/10.1038/nmat2297.

[2] Z.N. Yu, L. Tetard, L. Zhai, J.Y. Thomas, Supercapacitor electrode materials: nanostructures from 0 to 3 dimensions, Energy Environ. Sci. 8 (2015) 702–730. https://doi.org/10.1039/C4EE03229B.

[3] X. Shi, S. Zheng, Z.S. Wu, X. Bao, Recent advances of graphene-based materials for high-performance and new-concept supercapacitors. J. Energy Chem. 27 (2018) 25–42. https://doi.org/10.1016/j.jechem.2017.09.034.

[4] D.S. Achilleos, T.A. Hatton, Surface design and engineering of hierarchical hybrid nanostructures for asymmetric supercapacitors with improved electrochemical performance. J. Colloid Interface Sci. 447 (2015) 282–301. http://dx.doi.org/10.1016/j.jcis.2014.12.080.

[5] J. Wang, S. Dong, B. Ding, Y. Wang, X. Hao, H. Dou, Y. Xia, X. Zhang, Pseudocapacitive materials for electrochemical capacitors: from rational synthesis to capacitance optimization. Natl. Sci. Rev. 4 (2017) 71–90. https://doi.org/10.1093/nsr/nww072.

[6] Q. Meng, K. Cai, Y. Chen, L. Chen, Research progress on conducting polymer based supercapacitor electrode materials. Nano Energy 36 (2017) 268–285. https://doi.org/10.1016/j.nanoen.2017.04.040.

[7] C.J. Zhang, V. Nicolosi, Graphene and MXene-based transparent conductive electrodes and supercapacitors. Energy Storage Mater. 222 (2018) 11–20. doi:10.1016/j.ensm.2018.05.003.

[8] W. Zuo, R. Li, C. Zhou, Y. Li, J. Xia, J. Liu, 2017. Battery-supercapacitor hybrid devices: recent progress and future prospects. Adv. Sci. 4, 1600539. https://doi.org/10.1002/advs.201600539.

[9] M.S. Wu, H.H. Hsieh, Nickel oxide/hydroxide nanoplatelets synthesized by chemical precipitation for electrochemical capacitors. Electrochim. Acta 53 (2008) 3427–3435. https://doi.org/10.1016/j.electacta.2007.12.005.

[10] B. Zhao, L. Zhang, Q. Zhang, D. Chen, Y. Cheng, X. Deng, Y. Chen, R. Murphy, X. Xiong, B. Song, C.P. Wong, M.S. Wang, M. Liu, Rational design of Nickel Hydroxide-based nanocrystals on graphene for ultrafast energy storage. Adv. Energy Mater. 8 (2018) 1–10. doi:10.1002/aenm.201702247.

[11] D.M. MacArthur, The proton diffusion coefficient for the Nickel Hydroxide electrode. J. Electrochem. Soc. 117 (1970) 729–732. doi:10.1149/1.2407618.

[12] B. Anothumakkool, D. Guyomard, J. Gaubicher, L. Madec, Interest of molecular functionalization for electrochemical storage. Nano Res. 10 (2017) 4175–4200. doi:10.1007/s12274-017-1797-7.

[13] R. Gusmão, Z. Sofer, M. Pumera, Functional protection of exfoliated Black Phosphorus by noncovalent modification with anthraquinone, ACS Nano. 12 (2018) 5666–5673. doi:10.1021/acsnano.8b01474.

[14] P. Fortgang, T. Tite, V. Barnier, N. Zehani, C. Maddi, F. Lagarde, A.S. Loir, N. Jaffrezic-Renault, C. Donnet, F. Garrelie, C. Chaix, Robust electrografting on self-organized 3D graphene electrodes. ACS Appl. Mater. Interfaces. 8 (2016) 1424–1433. doi:10.1021/acsami.5b10647.

[15] D. Bélanger, J. Pinson, Electrografting: a powerful method for surface modification. Chem. Soc. Rev. 40 (2011) 3995–4048. doi:10.1039/C0CS00149J.

[16] P. Allongue, M. Delamar, B. Desbat, O. Fagebaume, R. Hitmi, J. Pinson, J.M. Savéant, Covalent modification of carbon surfaces by aryl radicals generated from the electrochemical reduction of diazonium salts. J. Am. Chem. Soc. 119 (1997) 201–207. doi:10.1021/ja963354s.

[17] C. Benoit, D. Demeter, D. Bélanger, C. Cougnon, A redox-active binder for electrochemical capacitor electrodes. Angew. Chem. Int. Ed. 55 (2016) 5318–5321. doi: 10.1002/anie.201601395.

[18] B.D. Assresahegn, T. Brousse, D. Bélanger, Advances on the use of diazonium chemistry for functionalization of materials used in energy storage systems. Carbon 92 (2015) 362–381. doi:10.1016/j.carbon.2015.05.030.

[19] G. Pognon, T. Brousse, D. Bélanger, Effect of molecular grafting on the pore size distribution and the double layer capacitance of activated carbon for electrochemical double layer capacitors. Carbon 49 (2011) 1340–1348. doi:10.1016/j.carbon.2010.11.055.

[20] R.K. Shervedani, A. Amini, N. Sadeghi, Electrografting of thionine diazonium cation onto the graphene edges and decorating with Au nano-dendrites or glucose oxidase: Characterization and electrocatalytic applications, Biosens. Bioelectron. 77 (2016) 478–485. doi:10.1016/j.bios.2015.09.062.

[21] A.L. Eckermann, D.J. Feld, J.A. Shaw, T.J. Meade, Electrochemistry of redox-active self-assembled monolayers. Coord. Chem. Rev. 254 (2010) 1769–1802. https://doi.org/10.1016/j.ccr.2009.12.023.

[22] C. Ornelas, J. Ruiz, C. Belin, D. Astruc, Giant dendritic molecular electrochrome batteries with ferrocenyl and pentamethylferrocenyl termini. J. Am. Chem. Soc. 131 (2009) 590–601. https://doi.org/10.1021/ja8062343.

[23] D. Astruc, Electron-transfer processes in dendrimers and their implication in biology, catalysis, sensing and nanotechnology. Nat. Chem. 4 (2012) 255–267. https://doi.org/10.1038/nchem.1304.

[24] M. Yu, X. Feng, Thin-film electrode-based supercapacitors. Joule 3 (2019) 338–360. https://doi.org/10.1016/j.joule.2018.12.012.

[25] E. Sibottier, S. Sayen, F. Gaboriaud, A. Walcarius, Factors affecting the

preparation and properties of electrodeposited silica thin films functionalized with amine or thiol groups. Langmuir 22 (2006) 8366–8373. https://doi.org/10.1021/la060984r.

[26] C.J. Brinker, A.J. Hurd, P.R. Schunk, G.C. Frye, C.S. Ashley, Review of sol-gel thin film formation. J. Non-Cryst. Solids 147–148 (1992) 424–436. https://doi.org/10.1016/S0022-3093(05)80653-2.

[27] F. Qu, R. Nasraoui, M. Etienne, Y. Bon Saint Côme, A. Kuhn, J. Lenz, J. Gajdzik, R. Hempelmann, A. Walcarius, Electrogeneration of ultra-thin silica films for the functionalization of macroporous electrodes. Electrochem. Commun. 13 (2011) 138–142. https://doi.org/10.1016/j.elecom.2010.11.034.

[28] I. Mazurenko, M. Etienne, R. Ostermann, B. Smarsly, O. Tananaiko, V. Zaitsev, A. Walcarius, Controlled electro-assisted deposition of sol-gel bio-composite on electrospun platinum nanofibers. Langmuir 27 (2011) 7140–7147. https://doi.org/10.1021/la200069z.

[29] L. Fang, Q.Q. He, M.J. Zhou, J.P. Zhao, J.M. Hu, 2019. Electrochemically assisted deposition of sol–gel films on graphene nanosheets. Electrochem. Commun. 109, 106609. https://doi.org/10.1016/j.elecom.2019.106609.

[30] A. Walcarius, Mesoporous materials and electrochemistry. Chem. Soc. Rev. 42 (2013) 4098–4140. https://doi.org/10.1039/C2CS35322A.

[31] A. Walcarius, E. Sibottier, M. Etienne, J. Ghanbaja, Electrochemically assisted self-assembly of mesoporous silica thin films. Nat. Mater. 6 (2007) 602–608. https://doi.org/10.1038/nmat1951.

[32] A. Goux, M. Etienne, E. Aubert, C. Lecomte, J. Ghanbaja, A. Walcarius, Oriented mesoporous silica films obtained by electro-assisted self-assembly (EASA). Chem. Mater. 21 (2009) 731–741. https://doi.org/10.1021/cm8029664.

[33] N. Vilà, J. Ghanbaja, E. Aubert, A. Walcarius, Electrochemically assisted generation of highly ordered azide-functionalized mesoporous silica for oriented hybrid films. Angew. Chem. Int. Ed. 53 (2014) 2945–2950. https://doi.org/10.1002/anie.201309447.

[34] N. Vilà, J. Ghanbaja, A. Walcarius, 2016. Clickable bifunctional and vertically-aligned mesoporous silica films. Adv. Mater. Interfaces 3, 1500440. https://doi.org/10.1002/admi.201500440.

[35] N. Vilà, A. Walcarius, Electrochemical response of vertically-aligned, ferrocene-functionalized mesoporous silica films: effect of the supporting electrolyte. Electrochim. Acta 179 (2015) 304–314. https://doi.org/10.1016/j.electacta.2015.02.169.

[36] J. Wang, N. Vilà, A. Walcarius, Redox-active vertically aligned mesoporous silica thin films as transparent surfaces for energy storage applications. ACS Appl. Mater. Interface 12 (2020) 24262–24270. https://doi.org/10.1021/acsami.0c03650.

[37] C. Karman, N. Vilà, C. Despas, A. Walcarius, Indirect amperometric detection of non-redox ions using a ferrocene-functionalized and oriented mesoporous silica thin film on electrode. Electrochim. Acta 228 (2017) 659–666. https://doi.org/10.1016/j.electacta.2017.01.126.

[38] R. Shi, C. Han, H. Duan, L. Xu, D. Zhou, H. Li, J. Li, F. Kang, B. Li, G. Wang, 2018. Redox-active organic sodium anthraquinone-2-sulfonate (AQS) anchored on reduced graphene oxide for high-performance supercapacitors. Adv. Energy Mater. 8, 1802088. https://doi.org/10.1002/aenm.201802088.

[39] Y. Liu, B. Zhang, Q. Xu, Y. Hou, S. Seyedin, S. Qin, G.G. Wallace, S. Beirne, J.M. Razal, J. Chen, Development of graphene oxide/polyaniline inks for high performance flexible microsupercapacitors via extrusion printing. Adv. Funct. Mater. 28 (2018) 1706592. https://doi.org/10.1002/adfm.201706592.

[40] W.H. Low, P.S. Khiew, S.S. Lim, C.W. Siong, E.R. Ezeigwe, Recent development of mixed transition metal oxide and graphene/mixed transition metal oxide based hybrid nanostructures for advanced supercapacitors. J. Alloys Compd. 775 (2019) 1324e1356. https://doi.org/10.1016/j.jallcom.2018.10.102.

[41] P. Yadav, S. Chacko, G. Kumar, R. Ramapanicker, V. Verma, Click chemistry route to covalently link cellulose and clay. Cellulose 22 (2015) 1615–1624. https://doi.org/10.1007/s10570-015-0594-2.

[42] K. Parvez, R. Li, S.R. Puniredd, Y. Hernandez, F. Hinkel, S. Wang, X. Feng, K. Müllen, Electrochemically exfoliated graphene as solution-processable, highly conductive electrodes for organic electronics. ACS Nano 7 (2013) 3598–3606. https://doi.org/10.1021/nn400576v.

[43] L. Hu, X.Peng, Y. Li, L. Wang, K. Huo, L.Y.S. Lee, K.Y. Wong, P.K. Chu, Direct anodic exfoliation of graphite onto high-density aligned graphene for large capacity supercapacitors. Nano Energy 34 (2017) 515–523. https://doi.org/10.1016/j.nanoen.2017.03.007.

[44] K. Parvez, Z.Wu, R. Li, X. Liu, R. Graf, Exfoliation of graphite into graphene in aqueous solutions. J. Am. Chem. Soc. 136 (2014) 6083–6091. https://doi.org/10.1021/ja5017156.

[45] Z. Li, B. Tang, Mn_3O_4/nitrogen-doped porous carbon fiber hybrids involving multiple covalent interactions and open voids as flexible anodes for lithium-ion batteries, Green Chem. 19 (2017) 5862–5873. doi:10.1039/c7gc02786a.

[46] K. Xiao, D. Jiang, R. Amal, D.W. Wang, A 2D conductive organic–inorganic hybrid with extraordinary volumetric capacitance at minimal swelling, Adv. Mater. 30 (2018) 1–8. doi:10.1002/adma.201800400.

[47] A.C. Ferrari, J. Robertson, Resonant Raman spectroscopy of disordered, amorphous, and diamondlike carbon. Phys. Rev. B 64 (2001) 075414. https://doi.org/10.1103/PhysRevB.64.075414.

[48] K.N. Kudin, B. Ozbas, H.C. Schniepp, R.K. Prud'Homme, I.A. Aksay, R. Car,

Raman spectra of graphite oxide and functionalized graphene sheets. Nano Lett. 8 (2008) 36–41. https://doi.org/10.1021/nl071822y.

[49] A.L. Dendramis, E.W. Schwinn, R.P. Sperline, A surface-enhanced Raman scattering study of CTAB adsorption on copper. Surf. Sci. 134 (1983) 675–688. https://doi.org/10.1016/0039-6028(83)90065-1.

[50] L. Poltorak, G. Herzog, A. Walcarius, Electrochemically assisted generation of silica deposits using a surfactant template at liquid/liquid micro-interfaces. Langmuir 30 (2014) 11453-11463. https://doi.org/10.1021/la501938g.

[51] O. De Los Cobos, B. Fousseret, M. Lejeune, F. Rossignol, M. Dutreilh-Colas, C. Carrion, C. Boissière, F. Ribot, C. Sanchez, X. Cattoën, M. Wong Chi Man, J.O. Durand, Tunable multifunctional mesoporous silica microdots arrays by combination of inkjet printing, EISA, and click chemistry. Chem. Mater. 24 (2012) 4337−4342. https://doi.org/10.1021/cm3022769.

[52] J. Jiang, X. Li, P. Zhu, D. Li, X. Han, Q. Cui, H. Zhu, Effect of pressure on 4-toluenesulfonyl azide studied by Raman scattering and Synchrotron X-ray diffraction. J. Phys. Chem. C 121 (2017) 1032−1039. https://doi.org/10.1021/acs.jpcc.6b11016.

[53] L.J.A. Macedo, R.M. Iost, A. Hassan, K. Balasubramanian, F.N. Crespilho, Bioelectronics and interfaces using monolayer graphene, ChemElectroChem. 6 (2019) 31–59. doi:10.1002/celc.201800934.

[54] X. Wang, A. Vasileff, Y. Jiao, Y. Zheng, S.Z. Qiao, Electronic and structural engineering of carbon-based metal-free electrocatalysts for water splitting, Adv. Mater. 31 (2019) 1–8. doi:10.1002/adma.201803625.

[55] N. Moitra, P. Trens, L. Raehm, J.O. Durand, X. Cattoën, M. Wong Chi Man, Facile route to functionalized mesoporous silica nanoparticles by click chemistry. J. Mater. Chem. 21 (2011) 13476–13482. https://doi.org/10.1039/c1jm12066b.

[56] R. A. Decréau, J.P. Collman, A. Hosseini, Electrochemical applications. How click chemistry brought biomimetic models to the next level: electrocatalysis under controlled rate of electron transfer. Chem. Soc. Rev. 39 (2010) 1291–1301. https://doi.org/10.1039/B901972N.

[57] L. Zhang, N. Vilà, G.W. Kohring, A. Walcarius, M. Etienne, Covalent immobilization of (2,2'-bipyridyl) (pentamethylcyclopentadienyl)-rhodium complex on a porous carbon electrode for efficient electrocatalytic NADH regeneration. ACS Catal. 7 (2017) 4386–4394. https://doi.org/10.1021/acscatal.7b00128.

[58] E. Piccinini, J.S. Tuninetti, J.I. Otamendi, S.E. Moya, M. Ceolín, F. Battaglini, O. Azzaroni, Surfactants as mesogenic agents in layer-by-layer assembled polyelectrolyte/surfactant multilayers: nanoarchitectured "soft" thin films displaying a tailored mesostructure. Phys. Chem. Chem. Phys. 20 (2018) 9298–9308.

https://doi.org/10.1039/C7CP08203G.

[59] J.F. Moulder, W.F. Stickle, P.E. Sobol, K.D. Bomben, Handbook of X-Ray Photoelectron Spectroscopy, Perkin-Elmer Corp, Eden Prairie, Minnesota, USA, 1992.

[60] E.W. Wollman, D. Kang, C.D. Frisbie, I. M. Lorkovic, M.S. Wrighton, Photosensitive self-assembled monolayers on gold: photochemistry of surface-confined aryl azide and cyclopentadienylmanganese tricarbonyl. J. Am. Chem. Soc. 116 (1994) 4395–4404. https://doi.org/10.1021/ja00089a030.

[61] J.P. Collman, N.K. Devaraj, T.P.A. Eberspacher, C.E.D. Chidsey, Mixed azide-terminated monolayers: a platform for modifying electrode surfaces. Langmuir 22 (2006) 2457–2464. https://doi.org/10.1021/la052947q.

[62] C.M. Woodbridge, D.L. Pugmire, R.C. Johnson, N.M. Boag, M.A. Langell, HREELS and XPS studies of ferrocene on Ag(100), J. Phys. Chem. B. 104 (2000) 3085–3093.

[63] A. Ambrosi, M. Pumera, Exfoliation of layered materials using electrochemistry, Chem. Soc. Rev. 47 (2018) 7213–7224. doi:10.1039/c7cs00811b.

[64] Z.M. Wang, W. Wang, N. Coombs, N. Soheilnia, G.A. Ozin, Graphene oxide-periodic mesoporous silica sandwich nanocomposites with vertically oriented channels. ACS Nano. 5 (2010) 7437–7450. https://doi.org/10.1021/nn102618n.

[65] D.M. Oliveira, A.S. Andrada, Synthesis of ordered mesoporous silica MCM-41 with controlled morphology for potential application in controlled drug delivery systems. Ceramica 65 (2019) 170–179.

[66] J. Yang, S. Gunasekaran, Electrochemically reduced graphene oxide sheets for use in high performance supercapacitors, Carbon 51 (2013) 36–44. doi:10.1016/j.carbon.2012.08.003.

[67] E.F. Dalton, N.A. Surridge, J.C. Jernigan, K.O. Wilbourn, J.S. Facci, R.W. Murray, Charge transport in electroactive polymers consisting of fixed molecular redox sites. Chem. Phys. 141 (1990) 143-157. https://doi.org/10.1016/0301-0104(90)80026-T.

[68] D.N. Blauch, J.M. Savéant, Dynamics of electron hopping in assemblies of redox centers. Percolation and diffusion. J. Am. Chem. Soc. 114 (1992) 3323–3332. https://doi.org/10.1021/ja00035a025.

[69] R. Pietschnig, Polymers with pendant ferrocenes. Chem. Soc. Rev. 45 (2016) 5216–5231. https://doi.org/10.1039/c6cs00196c.

[70] M.R. Lukatskaya, S. Kota, Z. Lin, M.Q. Zhao, N. Shpigel, M.D. Levi, J. Halim, P.L. Taberna, M.W. Barsoum, P. Simon, Y. Gogotsi, Ultra-high-rate pseudocapacitive energy storage in two-dimensional transition metal carbides. Nat. Energy 6 (2017) 1–6. https://doi.org/10.1038/nenergy.2017.105.

[71] J. Yang, X. Duan, Q. Qin, W. Zheng, Solvothermal synthesis of hierarchical flower-like β-NiS with excellent electrochemical performance for supercapacitors. J. Mater. Chem. A 1 (2013) 7880–7884. https://doi.org/10.1039/c3ta11167a.

[72] P. Si, S.Ding, X.W. Lou, D.H. Kim, An electrochemically formed three-dimensional structure of polypyrrole/graphene nanoplatelets for high-performance supercapacitors. RSC Adv. 1 (2011) 1271–1278. https://doi.org/10.1039/c1ra00519g.

[73] M. Zhi, A. Manivannan, F. Meng, N. Wu, Highly conductive electrospun carbon nanofiber/MnO_2 coaxial nano-cables for high energy and power density supercapacitors. J. Power Sources 208 (2012) 345–353. https://doi.org/10.1016/j.jpowsour.2012.02.048.

[74] Y. Yoon, K. Lee, S. Kwon, S. Seo, H. Yoo, S. Kim, Y. Shin, Y. Park, D. Kim, J.Y. Choi, H. Lee, Vertical alignments of graphene sheets spatially and densely piled for fast ion diffusion in compact supercapacitors. ACS Nano 8 (2014) 4580–4590. https://doi.org/10.1021/nn500150j.

[75] L. Liu, H. Zhao, Y. Wang, Y. Fang, J. Xie, Y. Lei, Evaluating the role of nanostructured current collectors in energy storage capability of supercapacitor electrodes with thick electroactive materials layers. Adv. Funct. Mater. 28 (2018) 1–9. https://doi.org/10.1002/adfm.201705107.

[76] W.W. Liu, Y.Q. Feng, X.B Yan, J.T. Chen, Q.J. Xue, Superior micro-supercapacitors based on graphene quantum dots. Adv. Funct. Mater. 23 (2013) 4111–4122. https://doi.org/10.1002/adfm.201203771.

[77] M.C. Henstridge, C. Batchelor-Mcauley, R. Gusmão, R.G. Compton, Marcus-Hush-Chidsey theory of electron transfer to and from species bound at a non-uniform electrode surface: Theory and experiment, Chem. Phys. Lett. 517 (2011) 108–112. doi:10.1016/j.cplett.2011.10.023.

[78] A. Afif, S.M.H. Rahman, A.T. Azad, J. Zaini, M.A.Islan, A.K. Azad. Advanced materials and technologies for hybrid supercapacitors for energy sorage – A review. J. Energy Storage 25 (2019) 100852. https://doi.org/10.1016/j.est.2019.100852.

[79] X. Wang, C. Yan, A. Sumboja, P.S. Lee, High performance porous nickel cobalt oxide nanowires for asymmetric supercapacitor, Nano Energy. 3 (2014) 119–126. doi:10.1016/j.nanoen.2013.11.001.

TOC entry

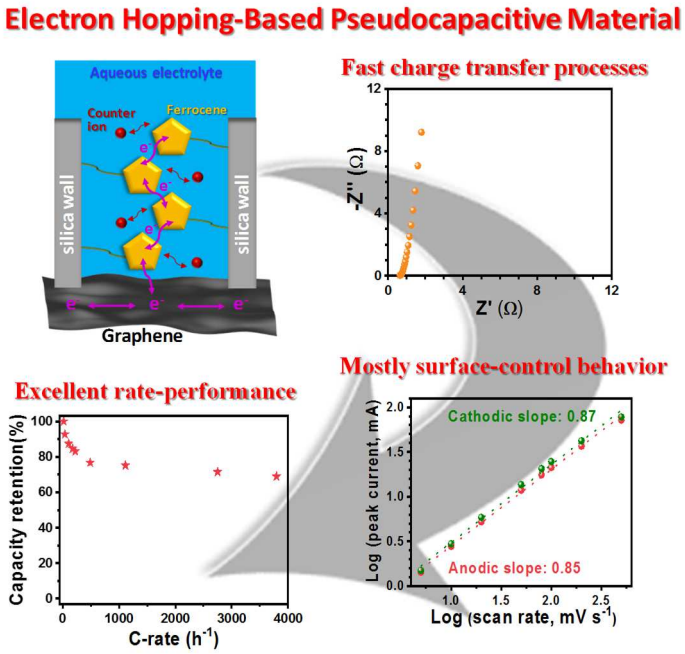
Electron Hopping-Based Pseudocapacitive Material
Aqueous electrolyte
Counter Ion
Ferrocene
silica wall
silica wall
Graphene
Fast charge transfer processes
-Z'' (Ω)
Z' (Ω)
Mostly surface-control behavior
Cathodic slope: 0.87
Anodic slope: 0.85
Log (peak current, mA)
Log (scan rate, mV s-1)
Excellent rate-performance
Capacity retention(%)
C-rate (h-1)